Experimental Evidence for Three Universality Classes for Reaction Fronts in Disordered Flows

Séverine Atis,[1][*] Awadhesh Kumar Dubey,[1] Dominique Salin,[1] Laurent Talon,[1] Pierre Le Doussal,[2] and Kay Jörg Wiese[2]

[1]*FAST, CNRS, UPSud, UPMC, UMR 7608, Batiment 502, Campus Universitaire, 91405 Orsay, France*
[2]*CNRS-Laboratoire de Physique Théorique de l'Ecole Normale Supérieure, 24 rue Lhomond, 75005 Paris, France*

Self-sustained reaction fronts in a disordered medium subject to an external flow display self-affine roughening, pinning, and depinning transitions. We measure spatial and temporal fluctuations of the front in $1 + 1$ dimensions, controlled by a single parameter, the mean flow velocity. Three distinct universality classes are observed, consistent with the Kardar-Parisi-Zhang (KPZ) class for fast advancing or receding fronts, the quenched KPZ class (positive-qKPZ) when the mean flow approximately cancels the reaction rate, and the negative-qKPZ class for slowly receding fronts. Both qKPZ classes exhibit distinct depinning transitions, in agreement with the theory.

PACS numbers: 47.56.+r, 61.43.-j, 82.40.-g

Growing interfaces are ubiquitous in nature, appearing in situations as different as bacterial colonies [1], solidification [2], atomic layer deposition [3,4], liquid interfaces in porous media [5–7], or crack propagation in heterogeneous materials [8,9]. The formation of scale-free structures in these systems raises the important question of universality in out-of-equilibrium phenomena.

In this Letter, we consider the propagation of a reaction front inside a porous medium. Resulting from the balance between the molecular diffusion D_m and the reaction rate $\tilde{\alpha}$, autocatalytic reactions can develop a traveling front. In the absence of an externally imposed flow, the reaction front develops into a flat horizontal front, propagating with a constant velocity $V_\chi = \sqrt{D_m \tilde{\alpha}/2}$, and a stationary concentration profile of width $l_\chi = D_m/V_\chi$. When coupled with the heterogeneous flow field of the porous medium, the fronts become rough, and modify their behavior accordingly with the flow strength and mean orientation relative to the chemical reaction direction. They propagate either downstream or upstream, or can remain frozen over a range of counterflow rates, delimited by two distinct depinning transitions [10,11]. Until now, however, their universality classes have not been identified.

Using both experimental and numerical approaches, we investigate their spatial and temporal scaling over the whole range of the externally imposed flow. In the vicinity of both depinning points, these reaction fronts display transient static configurations with distinct morphologies depending on the front propagation direction, displayed in Fig. 1. We show that this is a well-controlled system which encompasses several universality classes.

Two important classes predicted by the theory, and discussed below, are (i) nonlinear stochastic growth governed by the (thermal) Kardar-Parisi-Zhang (KPZ) equation (1), and (ii) growth where both the nonlinearity and quenched disorder are present, described by the quenched

KPZ (qKPZ) equation (2). It divides into two subclasses, positive qKPZ and negative qKPZ, depending on the sign of the nonlinearity λ.

It has been difficult to find unambiguous experimental realizations, due to long-range effects, quenched disorder, and a mixing of (i) and (ii) [1,12–14]. Recently, experiments on turbulent liquid crystals [13,15] made a precise
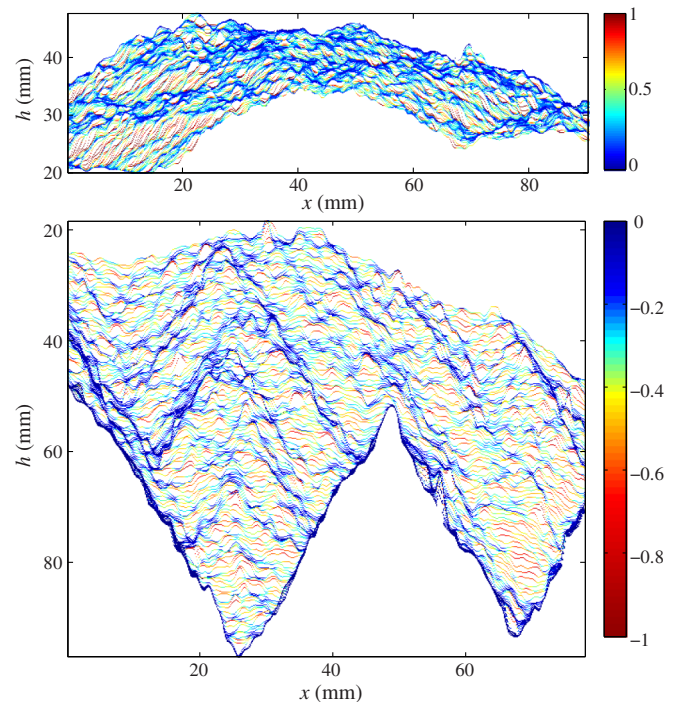

FIG. 1 (color online). Successive experimental fronts at constant time intervals. Color represents local front velocity, in units of imposed flow velocity $\bar{U}$. Top: upward propagating front near F_c^+ ($F = 0.56$). Bottom: backward propagating front near F_c^- ($F = -1.24$).

connection with the theory of the KPZ class experiencing a revolution of its own [16]. The (positive) qKPZ class [17,18] and both KPZ and qKPZ classes in evaporating colloidal suspensions [14] were observed. Remarkably, in the present system, by tuning a *single* parameter F, one can observe all *three* classes.

The KPZ equation [19] was proposed as a generic model for an interface growing along its local normal,

$$\frac{\partial h(x,t)}{\partial t} = \nu \nabla^2 h(x,t) + \frac{\lambda}{2}[\nabla h(x,t)]^2 + \eta(x,t) + f. \quad (1)$$

Its height $h(x,t)$ is along the vertical axis, ν an effective stiffness due to diffusion, λ the nonlinearity, and $\eta(x,t)$ a Gaussian white noise with $\overline{\eta(x,t)} = 0$ and $\overline{\eta(x,t)\eta(x',t')} = 2D\delta(x-x')\delta(t-t')$. f is an applied force, and up to a shift, proportional to the experimental applied force F as shown below. The surface can be characterized by two scaling exponents, the roughness α, and the growth exponent β, defined via $\overline{[h(x,t)-h(x',t)]^2} \sim |x-x'|^{2\alpha}$ and $\overline{[h(x,t)-h(x,t')]^2} \sim |t-t'|^{2\beta}$. In $d = 1+1$ dimensions, $\alpha_{\mathrm{KPZ}} = 1/2$ and $\beta_{\mathrm{KPZ}} = 1/3$ [19].

In a heterogeneous medium, the "noise" acquires a static *quenched* component, described by the qKPZ equation [20]:

$$\frac{\partial h(x,t)}{\partial t} = \nu \nabla^2 h(x,t) + \frac{\lambda}{2}[\nabla h(x,t)]^2 + \bar{\eta}(x,h(x,t)) + f. \quad (2)$$

The case $\lambda = 0$ models a number of systems, and is a distinct universality class (quenched Edwards-Wilkinson) [21] but does not seem to be relevant here (it predicts $\beta \approx 0.87$ and $\alpha > 1$.) In the KPZ equation (1) one can eliminate the driving by setting $h(x,t) = ft + \tilde{h}(x,t)$. Changing then $\tilde{h}(x,t) \rightarrow -\tilde{h}(x,t)$ reverses the sign of the nonlinear term λ, which is thus unimportant. By contrast, the qKPZ equation (2) does not allow for this change, since the term $\bar{\eta}[x,h(x,t)]$ is not invariant. The driving force f is thus a new parameter of the problem, and its sign (relative to the sign of λ) matters. If the disorder is statistically invariant by parity, i.e., if $\bar{\eta}(x,-h)$ has the same properties as $\bar{\eta}(x,h)$, Eq. (2) is invariant under $f \rightarrow -f$, $h(x,t) \rightarrow -h(x,t)$, and $\lambda \rightarrow -\lambda$, leading to two cases: Positive qKPZ when λ and f have the same sign, and negative qKPZ when they have opposite sign.

In the moving phase, qKPZ of either sign crosses over to KPZ at large scales. This is seen, e.g., in the limit of large mean interface velocity $v = \overline{\partial_t h(x,t)}$: Consider Eq. (2) with white noise $\overline{\bar{\eta}(x,h)\bar{\eta}(x',h')} = 2\bar{D}\delta(x-x')\delta(h-h')$ and perform the change $h(x,t) \rightarrow vt + \tilde{h}(x,t)$. The disorder then becomes

$$\bar{\eta}(x,vt+\tilde{h}(x,t)) \approx \bar{\eta}(x,vt), \quad (3)$$

i.e., the same noise as in the KPZ equation (1), identifying $D = \bar{D}/v$. As v is decreased, the crossover from qKPZ at short scales to KPZ occurs at larger and larger scales.

The positive qKPZ equation exhibits a depinning transition [20,22], well characterized in $d = 1+1$. The mean interface velocity vanishes for $f < f_c^+$; for $f > f_c^+$ it moves with velocity $v \sim (f-f_c^+)^\theta$. At f_c the pinned interface outlines a transversal path on a directed percolation (DP) cluster [17,18,23] with roughness $\alpha_{\mathrm{DP}} \simeq 0.63$, and a growth exponent $\beta_{\mathrm{DP}} \simeq 0.63$. As discussed above, the quenched nature of the noise is relevant only when f is close to f_c.

The predictions for the negative qKPZ class are different [24]. In the pinned phase, $\lambda > 0$ and negative $f > f_c^-$, the interface forms sawtooth configurations (see Fig. 1, bottom) where alternating nonzero local average slopes $|\nabla h|$ help the system to remain pinned. As f decreases, the sawtooth slopes increase until there are discontinuous jumps at f_c^- of both the average slope (back to zero) and the velocity v, well evident in our experiment; see Fig. 2(a). Inside the pinned phase, the transitory dynamics is similar to positive qKPZ [25], and the depinning was analyzed via a mapping to the first layer Polynuclear growth (PNG) model [26], a close cousin of KPZ.

Our experiment is made with the iodate arsenous acid reaction, autocatalytic in iodide, with the concentration values $[\mathrm{IO}_3^-] = 7.5$ mM and $[\mathrm{H}_3\mathrm{AsO}_3]_0 = 25$ mM, such that the arsenous acid is in excess [27,28]. The resulting front has a velocity $V_\chi \simeq 11.2$ μm/s, and a width
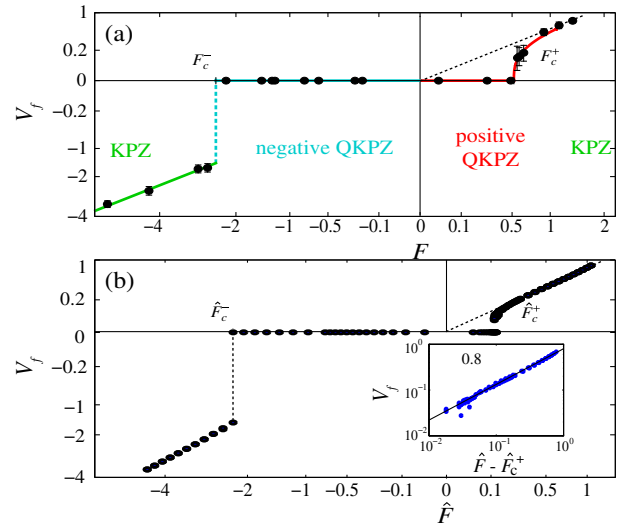

FIG. 2 (color online). Front velocity V_f versus the applied force F ($\hat{F}$), in adverse flow (a) experiments (black dots with error bars), (b) numerics. Dashed lines are linear extrapolation of the advancing branch. To put all data on one plot, axes are rescaled according to $F \rightarrow F/|F|^{1/2}$, $V_f \rightarrow V_f/|V_f|^{1/2}$. Inset: front velocity versus $\hat{F} - \hat{F}_{c^+}$. The continuous line corresponds to $v(\hat{F}) \propto (\hat{F} - \hat{F}_{c^+})^{0.8\pm0.05}$.

$l_\chi \simeq 200~\mu$m. The front position is visualized with polyvinyl alcohol colored by transient iodine production [29]. The disordered flow is generated with a 50% mixture of 1.5 and 2 mm diameters packed glass beads inside a transparent ($300 \times 100 \times 4$ mm^3) rectangular cell. A range of injectors at the top of the cell can either suck out or inject unreacted fluid parallel to the vertical. The bottom of the cell is dipped into a container with reacted solution to start the reaction, leading to a flat horizontal initial front. The front propagates upwards in the absence of the flow, which is then switched on once the desired vertical position is reached. We extract the location $h(x, t)$ of the front at a given position x and time t from 700×1000 pixel digitized images with a 12-bit Roper Coolsnap HQ video camera. To enhance the statistics, we performed 3 to 6 different realizations for each of the 30 values of the applied flow velocity.

We define the control parameter as $F = (\bar{U} + V_\chi)/V_\chi + f_0$, with $\bar{U}$ the mean flow velocity and $f_0 \simeq 0.38$ an *ad hoc* constant [30], such that the front advances when $F > 0$ or recedes when $F < 0$. Figure 2(a) displays the normalized front velocity, $v = V_f/V_\chi$ as a function of F. In the absence of flow, when $F = 1 + f_0$, the reaction front propagates through the beads with a smooth shape at a constant velocity $V_f = V_0 = 0.8 V_\chi \pm 0.5~\mu$m/s (see Supplemental Material [30], movie 1). When the flow is turned on, the front exhibits distinct self-affine scalings depending on F, and quantified by the front width $w(\Delta x) \sim (\Delta x)^\alpha$, and the standard deviation of the temporal height fluctuations $w(\Delta t) \sim (\Delta t)^\beta$ [30,31].

At large flow rates, when $|F| > 2.5$ in Fig. 2, V_f is a linear function of F and the front propagates downstream for both orientations of the mean flow (see Supplemental Material [30], movies 2 and 3). Figure 3(a) shows the width $w(\Delta x)$ and $w(\Delta t)$ of saturated fronts, i.e., such that $\ell^*(t) \sim L$ [31], determined for experiments realized at opposite mean-flow orientations. They display both a similar
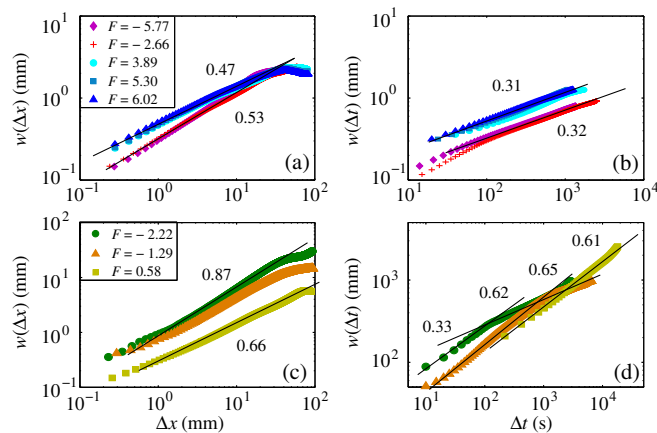
roughness $\alpha = 0.47 \pm 0.03$, and $\alpha = 0.53 \pm 0.04$, and growth exponent $\beta = 0.32 \pm 0.04$ and $\beta = 0.37 \pm 0.05$ while $t^* \approx T$. As can be seen in Fig. 4(a), at large front velocity of either orientation, the front exhibits scale-invariant fluctuations with statistical properties in agreement with the KPZ class and the theoretical discussion around Eq. (3). In addition, since in the experiment $\bar{D} \sim V_f$, the expected KPZ noise $D \simeq \bar{D}/V_f$ is almost independent of V_f [30], and the amplitude of $w(\Delta x)$ does not vary significantly with F for a given flow orientation, as can be seen in Fig. 3(a).

When $F \to 0$, some regions of the front pin to the flow heterogeneities. In this configuration, the front propagates mainly upstream, from the bottom to the top of the cell, while locally the front exhibits transiently static regions, as shown in Fig. 1 (top). Note that the moving parts have a larger slope than the arrested or slowly propagating ones, leading to a lateral growth of the fronts in this regime (Supplemental Material [30], movie 4). When the opposite flow is amplified, the pinned portions become larger. The value F_{c^+} for which the front eventually stops and remains static is $F_{c^+} = 0.56 \pm 0.05$. In Figs. 3(c) and 3(d) for $F = 0.58$, the values $\alpha = 0.66 \pm 0.04$ and $\beta = 0.61 \pm 0.05$, are consistent with the theoretically predicted exponents of positive qKPZ, $\alpha = \beta = 0.63$ (see Ref. [30] for additional measurements), suggesting that the front undergoes a depinning transition when $F \to F_{c^+}$.

Finally, when F decreases below F_{c^+}, the transient front propagation becomes very short. For $F \approx 0$, the front is static almost instantaneously after the flow is turned on (Supplemental Material [30], movie 5). When F becomes negative, the front propagates in the direction opposite to the chemical reaction. For sufficiently small F, $-2.22 \lesssim F \lesssim 0$, it quickly becomes static after a transient propagation and displays a particular sawtooth pattern [10]. One notes in Fig. 1(b) that the front is slowed down or arrested when it reaches a certain slope, resulting in facet formation (Supplemental Material [30], movie). Another depinning transition occurs at $F_{c^-} \approx -2.22 \pm 0.05$, below which triangular states become unstable and the front goes back to a phase moving from the top to the bottom of the

FIG. 3 (color online). Height fluctuations of the front. Left column: roughness $w(\Delta x)$ and right column: temporal fluctuations $w(\Delta t)$. (a) and (b) for $|F| > 2.5$; (c) and (d) for $|F| < 2.5$.
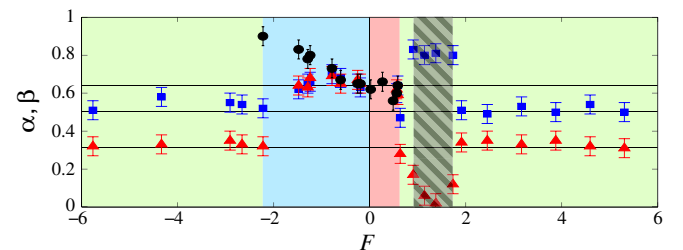

FIG. 4 (color online). Experimental exponents versus F. Roughness exponent α (blue squares), and growth exponent β (red triangles) for moving fronts. Roughness of the pinned fronts (black circles). Hatched region corresponds to weak noise when $\bar{U} \to 0$.

cell. As indicated in Fig. 4, these triangular shapes lead to a different roughness exponent of the transiently moving parts compared to the final static front as $F \to F_{c^-}$ [30]. The roughness and growth exponents of propagating regions have $0.62 \lesssim \alpha \lesssim 0.7$ and $0.63 \lesssim \beta \lesssim 0.69$, consistent with the observations in Ref. [25]. However, the final static front roughness is larger: $0.73 \lesssim \alpha \lesssim 0.9$, increasing as the sawtooth slope rises when $F \to F_{c^-}$. Interestingly, a crossover from $\beta \approx 0.65$ to $\beta \approx 0.33$ for larger scales is visible in Fig. 3(d), underlining the second depinning transition at F_{c^-}. Close to F_{c^-}, the front pins to pointlike regions, while close to F_{c^+} the pinning regions extend horizontally. This shows that receding fronts are consistent with negative qKPZ, known for similar pinning processes and interface morphologies [24,26,32]. This model also predicts a first-order depinning transition, observed here as a jump in the $V_f(F)$ curve.

To better understand the behavior close to the transitions, lattice Boltzmann simulations were performed in a 2D disordered porous medium (2048×2048 grid size), solving the convection-diffusion reaction and the Darcy-Brinkman equations [11,30,33]. Figure 2(b) displays the numerical front velocity versus $\hat{F} = (\bar{U} + V_\chi)/V_\chi + \hat{f}_0$, where hatted quantities denote parameters in the simulations with $\hat{f}_0 = 0.256$. In good agreement with the experiments, two transitions occur at $\hat{F}_{c^-} = -2.2 \pm 0.2$ and $\hat{F}_{c^+} = 0.095 \pm 0.015$ and the velocity $V_f(\hat{F})$ is almost linear in $\hat{F}$ below the first transition and beyond the second one. While the transition at $\hat{F}_{c^-}$ is very abrupt, the second one at $\hat{F}_{c^+}$ is more continuous. Moreover, the critical behavior can be fitted [Fig. 2(b), inset] with a power law $V_f(\hat{F}) \sim (\hat{F} - \hat{F}_{c^+})^{0.8 \pm 0.05}$, with an exponent slightly larger than the theoretical value 0.66 [17]. This is consistent with a first-order transition at $\hat{F}_{c^-}$ and a second-order one at $\hat{F}_{c^+}$. Shown in Fig. 5, the scaling exponents of the numerics are also in good agreement with the theory of the thermal KPZ class for large $|\hat{F}|$. Near the depinning transitions at $\hat{F}_{c^+}$ and $\hat{F}_{c^-}$, the roughness exponents $\alpha = 0.65 \pm 0.05$ and $\alpha = 0.9 \pm 0.05$ are consistent with experiments and the positive and negative qKPZ predictions. The remaining differences in the qKPZ pinned phase are due to different initial conditions: In the experiment, the fronts propagate without flow (with their own roughness exponent at $\bar{U} = 0$) and then the flow is switched on, whereas in the simulation the
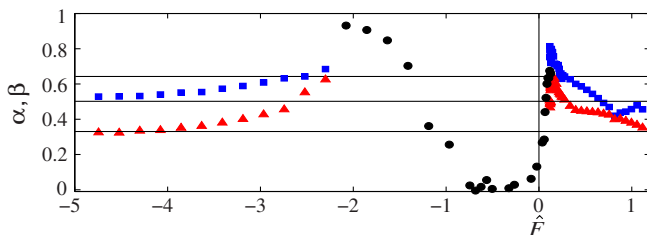
initial front is flat (see Supplemental Material [30] for details).

The good agreement between experiments, numerical simulations, and theory for the different KPZ universality classes can be understood through the *eikonal* approximation [34,35]. For a thin front, the local front velocity follows the eikonal equation: $\vec{V}_f \cdot \vec{n} = V_\chi + D_m \kappa + \vec{U}(\vec{r}) \cdot \vec{n}$, where $\vec{n}$ is the normal of the front, κ the curvature, and $\vec{U}(\vec{r})$ the local flow velocity. Indeed, this equation is similar to the "flux-line model" of Kardar [36], where the chemical velocity plays the role of the Lorentz force, and the disordered flow that of the random force. After projection and neglecting higher-order terms [30], the eikonal approximation yields

$$\frac{\partial h}{\partial t} \simeq V_\chi \sqrt{1 + (\nabla h)^2} + \frac{D_m \nabla^2 h}{1 + (\nabla h)^2} + \bar{U} + \delta U_y(\vec{r}). \quad (4)$$

Assuming small gradients, and normalizing by V_χ, leads to Eq. (2) where $\bar{\eta} \equiv \delta U_y$ and with the parameters $\nu = l_\chi = D_m/V_\chi$, $\lambda = 1$, and $f = (\bar{U} + V_\chi)/V_\chi$, whose small renormalization due to the neglected terms can be estimated [37]. The difference $F - f = f_0$ is related to the space average of the KPZ term $f_0 \sim (\lambda/2)\langle(\nabla h)^2\rangle_L$. Note that $\lambda = 1$ is independent of the front propagation direction, and fixed by the initial condition of the experiment. Negative qKPZ describes then the backward moving fronts, i.e., $\partial h/\partial t < 0$, since performing $h \to -h$ is equivalent to measuring the front position along the $-\hat{y}$ axis. Finally, near the transition at F_{c^-}, the slope of the sawtooths may be large. Although it correctly predicts the first-order transition, small-gradient qKPZ may not be quantitatively accurate. A more precise scenario was proposed in [38], based on the PNG model [26] and extreme-value statistics.

In conclusion, chemical-wave propagation coupled with the disordered flow in a porous medium, develop self-affine structures, with scaling exponents consistent with either KPZ or qKPZ classes. Remarkably, by tuning a single parameter, this system passes through three universality classes, providing a rich experimental setting to study growth phenomena. Slowly backward propagating fronts constitute beautiful experimental evidence of a chemical interface described by negative qKPZ. Part of this phenomenology was recently observed in magnetic domain walls [32]: it would be interesting to reach the thermal KPZ class there by increasing the driving. This work opens the door for further investigations on frozen pattern formation in out-of-equilibrium systems [39].

FIG. 5 (color online). Roughness and growth exponents in the simulations. Same symbols as in Fig. 4.

*Corresponding author.
Present address: Department of Mechanical Engineering, Massachusetts Institute of Technology, Cambridge, Massachusetts 02139, USA.
atis@mit.edu

[1] M. A. C. Huergo, M. A. Pasquale, A. E. Bolzan, A. J. Arvia, and P. H. Gonzalez, Phys. Rev. E **82**, 031903 (2010).

[2] J. S. Langer, Rev. Mod. Phys. **52**, 1 (1980).

[3] R. Messier and J. E. Yehoda, J. Appl. Phys. **58**, 3739 (1985).

[4] J. Wakita, H. Itoh, T. Matsuyama, and M. Matsushita, J. Phys. Soc. Jpn. **66**, 67 (1997).

[5] D. Wilkinson and J. F. Willemsen, J. Phys. A **16**, 3365 (1983).

[6] V. K. Horvath, F. Family, and T. Vicsek, J. Phys. A **24**, L25 (1991).

[7] S. Santucci, R. Planet, K. J. Maloy, and J. Ortin, Europhys. Lett. **94**, 46005 (2011).

[8] E. Bouchaud, J. Phys. Condens. Matter **9**, 4319 (1997).

[9] K. J. Maloy and J. Schmittbuhl, Phys. Rev. Lett. **87**, 105502 (2001).

[10] S. Atis, S. Saha, H. Auradou, D. Salin, and L. Talon, Phys. Rev. Lett. **110**, 148301 (2013).

[11] S. Saha, S. Atis, D. Salin, and L. Talon, Europhys. Lett. **101**, 38003 (2013).

[12] J. Maunuksela, M. Myllys, O. P. Kahkonen, J. Timonen, N. Provatas, M. J. Alava, and T. Ala-Nissila, Phys. Rev. Lett. **79**, 1515 (1997).

[13] K. A. Takeuchi and M. Sano, Phys. Rev. Lett. **104**, 230601 (2010).

[14] P. J. Yunker, M. A. Lohr, T. Still, A. Borodin, D. J. Durian, and A. G. Yodh, Phys. Rev. Lett. **110**, 035501 (2013); M. Nicoli, R. Cuerno, and M. Castro, Phys. Rev. Lett. **111**, 209601 (2013); P. J. Yunker, M. A. Lohr, T. Still, A. Borodin, D. J. Durian, and A. G. Yodh, Phys. Rev. Lett. **111**, 209602 (2013).

[15] K. A. Takeuchi, J. Stat. Mech. (2014) P01006.

[16] I. Corwin, arXiv:1106.1596, and references therein.

[17] L. A. N. Amaral, A. L. Barabasi, S. V. Buldyrev, S. T. Harrington, S. Havlin, R. Sadr-Lahijany, and H. E. Stanley, Phys. Rev. E **51**, 4655 (1995).

[18] S. V. Buldyrev, A. L. Barabasi, F. Caserta, S. Havlin, H. E. Stanley, and T. Vicsek, Phys. Rev. A **45**, R8313 (1992).

[19] M. Kardar, G. Parisi, and Y. C. Zhang, Phys. Rev. Lett. **56**, 889 (1986).

[20] D. A. Kessler, H. Levine, and Y. Tu, Phys. Rev. A **43**, 4551 (1991).

[21] H. Leschhorn, T. Nattermann, S. Stepanow, and L.-H. Tang, Ann. Phys. (N.Y.) **509**, 1 (1997); For reviews, see K. Wiese and P. Le Doussal, Markov Processes Relat. Fields **13**, 777 (2007); P. Le Doussal, Int. J. Mod. Phys. B **24**, 3855 (2010).

[22] G. Parisi, Europhys. Lett. **17**, 673 (1992).

[23] L. H. Tang and H. Leschhorn, Phys. Rev. A **45**, R8309 (1992).

[24] H. Jeong, B. Kahng, and D. Kim, Phys. Rev. Lett. **77**, 5094 (1996); Phys. Rev. E **59**, 1570 (1999).

[25] Y. M. Choi, H. J. Kim, and I. M. Kim, Phys. Rev. E **66**, 047102 (2002).

[26] G. J. Szabo and M. J. Alava, Physica (Amsterdam) **301A**, 17 (2001).

[27] A. Hanna, A. Saul, and K. Showalter, J. Am. Chem. Soc. **104**, 3838 (1982).

[28] M. Leconte, J. Martin, N. Rakotomalala, and D. Salin, Phys. Rev. Lett. **90**, 128302 (2003).

[29] I. B. Malham, N. Jarrige, J. Martin, N. Rakotomalala, L. Talon, and D. Salin, J. Chem. Phys. **133**, 244505 (2010).

[30] See Supplemental Material at http://link.aps.org/supplemental/10.1103/PhysRevLett.114.234502 for the experimental and numerical methods.

[31] We define $w(\Delta x) = \langle \sqrt{\langle [h(x,t) - \langle h \rangle_{\Delta x}]^2 \rangle_{\Delta x}} \rangle_{x,t}$; here $\langle \rangle_{\Delta x}$ represents an average over a length Δx, and $\langle \rangle_{x,t}$ a translational average over x, as well as a temporal average over time t, in the steady state. Temporal fluctuations are quantified by $w(\Delta t) = \langle \sqrt{\langle [h(x,t) - \langle h(t) \rangle_x]^2 \rangle_{\Delta t}} \rangle_{x,t}$, where Δt is a time window. Both quantities exhibit power laws, $w(\Delta x) \sim \Delta x^{\alpha}$ for $\Delta x \ll \ell^*(t)$, and $w(\Delta t) \sim \Delta t^{\beta}$ for $\Delta t \ll t^*(L)$, with $\ell^*(t)$ and $t^*(L)$ the spatial and temporal correlation lengths.

[32] K. W. Moon, D. H. Kim, S. C. Yoo, C. G. Cho, S. Hwang, B. Kahng, B. C. Min, K. H. Shin, and S. B. Choe, Phys. Rev. Lett. **110**, 107203 (2013).

[33] L. Talon, J. Martin, N. Rakotomalala, D. Salin, and Y. Yortsos, Water Resour. Res. **39**, 1135 (2003).

[34] B. F. Edwards, Phys. Rev. Lett. **89**, 104501 (2002).

[35] B. F. Edwards, Chaos **16**, 043106 (2006).

[36] M. Kardar, Phys. Rep. **301**, 85 (1998).

[37] P. Le Doussal and K. J. Wiese, Phys. Rev. E **67**, 016121 (2003).

[38] T. Gueudré, A. K. Dubey, L. Talon, and A. Rosso, Phys. Rev. E **89**, 041004 (2014).

[39] V. Schaller, C. A. Weber, B. Hammerich, E. Frey, and A. R. Bausch, Proc. Natl. Acad. Sci. U.S.A. **108**, 19183 (2011); P. Le Doussal and T. Giamarchi, Phys. Rev. B **57**, 11356 (1998).